Bendable, ultra-black absorber based on a graphite nanocone nanowire composite structure

Yaoran Sun,[1] Julian Evans,[1,*] Fei Ding,[1] Nan Liu,[2] Wen Liu,[1] Yuan Zhang,[1] and Sailing He[1,3]

[1]*Centre for Optical and Electromagnetic Research, Zhejiang Provincial Key Laboratory for Sensing Technologies, Zhejiang University, Hangzhou 310058, China*
[2]*Center for Integrated Optoelectronics, State Key Laboratory of Modern Optical Instrumentation, Zhejiang University, Hangzhou 310027, China*
[3]*Department of Electromagnetic Engineering, Royal Institute of Technology, S-100 44 Stockholm, Sweden*
[*]*Julian.Evans@colorado.edu*

Abstract: A bendable ultra-black material consisting of graphite nanocones and nanowires is fabricated through a simple plasma etching process. The optical properties of the absorber are characterized in the wavelength range of 400-2000 nm with average specular reflectance 0.05 ± 0.03% at normal incidence and the material thickness is only around 5 μm. The reflectance of the absorber remains low at large incident angles and is relatively independent of polarization. Simulations confirm the cooperative effect of the nanowires and nanocones leading to an ultra-black thin carbon material.

©2015 Optical Society of America

OCIS codes: (310.6628) Subwavelength structures, nanostructures; (310.6860) Thin films, optical properties.

References and links

1. A. Lenert, D. M. Bierman, Y. Nam, W. R. Chan, I. Celanović, M. Soljačić, and E. N. Wang, "A nanophotonic solar thermophotovoltaic device," Nat. Nanotechnol. **9**(2), 126–130 (2014).
2. T. Sato, N. Yoshizawa, and T. Hashizume, "Realization of an extremely low reflectance surface based on InP porous nanostructures for application to photoelectrochemical solar cells," Thin Solid Films **518**(15), 4399–4402 (2010).
3. A. Cao, X. Zhang, C. Xu, B. Wei, and D. Wu, "Tandem structure of aligned carbon nanotubes on Au and its solar thermal absorption," Sol. Energy Mater. Sol. Cells **70**(4), 481–486 (2002).
4. S. P. Theocharous, E. Theocharous, and J. H. Lehman, "The evaluation of the performance of two pyroelectric detectors with vertically aligned multi-walled carbon nanotube coatings," Infrared Phys. Technol. **55**(4), 299–305 (2012).
5. J. Lehman, E. Theocharous, G. Eppeldauer, and C. Pannell, "Gold-black coatings for freestanding pyroelectric detectors," Meas. Sci. Technol. **14**(7), 916–922 (2003).
6. J. G. Hagopian, S. A. Getty, M. Quijada, J. Tveekrem, R. Shiri, P. Roman, J. Butler, G. Georgiev, J. Livas, C. Hunt, A. Maldonado, S. Talapatra, X. Zhang, S. J. Papadakis, A. H. Monica, and D. Deglau, "Multiwalled carbon nanotubes for stray light suppression in space flight instruments," Proc. SPIE **7761**, 77610F (2010).
7. M. Steglich, D. Lehr, S. Ratzsch, T. Käsebier, F. Schrempel, E.-B. Kley, and A. Tünnermann, "An ultra-black silicon absorber," Laser Photonics Rev. **8**(2), L13–L17 (2014).
8. E. Theocharous, C. J. Chunnilall, R. Mole, D. Gibbs, N. Fox, N. Shang, G. Howlett, B. Jensen, R. Taylor, J. R. Reveles, O. B. Harris, and N. Ahmed, "The partial space qualification of a vertically aligned carbon nanotube coating on aluminium substrates for EO applications," Opt. Express **22**(6), 7290–7307 (2014).
9. R. J. C. Brown, P. J. Brewer, and M. J. T. Milton, "The physical and chemical properties of electroless nickel–phosphorus alloys and low reflectance nickel–phosphorus black surfaces," J. Mater. Chem. **12**(9), 2749–2754 (2002).
10. E. A. Taft and H. R. Philipp, "Optical properties of graphite," Phys. Rev. **138**(1A), A197–A202 (1965).
11. K. Mizuno, J. Ishii, H. Kishida, Y. Hayamizu, S. Yasuda, D. N. Futaba, M. Yumura, and K. Hata, "A black body absorber from vertically aligned single-walled carbon nanotubes," Proc. Natl. Acad. Sci. U.S.A. **106**(15), 6044–6047 (2009).
12. J. Lehman, A. Sanders, L. Hanssen, B. Wilthan, J. Zeng, and C. Jensen, "Very black infrared detector from vertically aligned carbon nanotubes and electric-field poling of lithium tantalate," Nano Lett. **10**(9), 3261–3266 (2010).

#242069 Received 1 Jun 2015; revised 20 Jul 2015; accepted 21 Jul 2015; published 24 Jul 2015

13. N. T. Panagiotopoulos, E. K. Diamanti, L. E. Koutsokeras, M. Baikousi, E. Kordatos, T. E. Matikas, D. Gournis, and P. Patsalas, “Nanocomposite catalysts producing durable, super-black carbon nanotube systems: applications in solar thermal harvesting,” ACS Nano **6**(12), 10475–10485 (2012).
14. N. Tomlin, A. Curtin, M. White, and J. Lehman, “Decrease in reflectance of vertically-aligned carbon nanotubes after oxygen plasma treatment,” Carbon **74**, 329–332 (2014).
15. H. Shi, J. G. Ok, H. W. Baac, and L. J. Guo, “Low density carbon nanotube forest as an index-matched and near perfect absorption coating,” Appl. Phys. Lett. **99**(21), 211103 (2011).
16. C. Chunnilall, J. Lehman, E. Theocharous, and A. Sanders, “Infrared hemispherical reflectance of carbon nanotube mats and arrays in the 5–50μm wavelength region,” Carbon **50**(14), 5348–5350 (2012).
17. N. Selvakumar, S. B. Krupanidhi, and H. C. Barshilia, “Carbon nanotube-based tandem absorber with tunable spectral selectivity: transition from near-perfect blackbody absorber to solar selective absorber,” Adv. Mater. **26**(16), 2552–2557 (2014).
18. Z.-P. Yang, L. Ci, J. A. Bur, S.-Y. Lin, and P. M. Ajayan, “Experimental observation of an extremely dark material made by a low-density nanotube array,” Nano Lett. **8**(2), 446–451 (2008).
19. X. Wang, L. Wang, O. Adewuyi, B. A. Cola, and Z. Zhang, “Highly specular carbon nanotube absorbers,” Appl. Phys. Lett. **97**(16), 163116 (2010).
20. S. Choi, H. Park, S. Lee, and K. H. Koh, “Fabrication of graphite nanopillars and nanocones by reactive ion etching,” Thin Solid Films **513**(1-2), 31–35 (2006).
21. H. Fredriksson, T. Pakizeh, M. Käll, B. Kasemo, and D. Chakarov, “Resonant optical absorption in graphite nanostructures,” J. Opt. A, Pure Appl. Opt. **11**(11), 114022 (2009).
22. H. Fredriksson, D. Chakarov, and B. Kasemo, “Patterning of highly oriented pyrolytic graphite and glassy carbon surfaces by nanolithography and oxygen plasma etching,” Carbon **47**(5), 1335–1342 (2009).
23. A. Savvatimskiy, “Measurements of the melting point of graphite and the properties of liquid carbon (a review for 1963–2003),” Carbon **43**(6), 1115–1142 (2005).
24. A. B. Kaul, J. B. Coles, M. Eastwood, R. O. Green, and P. R. Bandaru, “Ultra-high optical absorption efficiency from the ultraviolet to the infrared using multi-walled carbon nanotube ensembles,” Small **9**(7), 1058–1065 (2013).
25. L. Mo, L. Yang, A. Nadzeyka, S. Bauerdick, and S. He, “Enhanced broadband absorption in gold by plasmonic tapered coaxial holes,” Opt. Express **22**(26), 32233–32244 (2014).
26. J. Cai and L. Qi, “Recent advances in antireflective surfaces based on nanostructure arrays,” Mater. Horiz. **2**(1), 37–53 (2015).
27. M. S. Dresselhaus, A. Jorio, M. Hofmann, G. Dresselhaus, and R. Saito, “Perspectives on carbon nanotubes and graphene Raman spectroscopy,” Nano Lett. **10**(3), 751–758 (2010).
28. S. Ryu, J. Maultzsch, M. Y. Han, P. Kim, and L. E. Brus, “Raman spectroscopy of lithographically patterned graphene nanoribbons,” ACS Nano **5**(5), 4123–4130 (2011).
29. F. Garcia-Vidal, J. Pitarke, and J. Pendry, “Effective medium theory of the optical properties of aligned carbon nanotubes,” Phys. Rev. Lett. **78**(22), 4289–4292 (1997).
30. S. Ravipati, J. Shieh, F. H. Ko, C. C. Yu, and H. L. Chen, “Ultralow reflection from a-Si nanograss/Si nanofrustum double layers,” Adv. Mater. **25**(12), 1724–1728 (2013).
31. B. T. Draine, “Scattering by interstellar dust grains. I. optical and ultraviolet,” Astrophys. J. **598**(2), 1017–1025 (2003).
32. Y.-F. Huang, S. Chattopadhyay, Y.-J. Jen, C.-Y. Peng, T. A. Liu, Y.-K. Hsu, C.-L. Pan, H.-C. Lo, C.-H. Hsu, Y.-H. Chang, C.-S. Lee, K. H. Chen, and L. C. Chen, “Improved broadband and quasi-omnidirectional anti-reflection properties with biomimetic silicon nanostructures,” Nat. Nanotechnol. **2**(12), 770–774 (2007).
33. Y.-F. Huang, Y.-J. Jen, L.-C. Chen, K.-H. Chen, and S. Chattopadhyay, “Design for approaching cicada-wing reflectance in low- and high-index biomimetic nanostructures,” ACS Nano **9**(1), 301–311 (2015).
34. Y.-F. Huang and S. Chattopadhyay, “Nanostructure surface design for broadband and angle-independent antireflection,” J. Nanophotonics **7**(1), 073594 (2013).

---

1. Introduction

Ultra-black materials that absorb almost all incoming radiation are important in many fields such as solar energy collectors, pyroelectric sensors, and stray light shields in optical systems [1–8]. Ultra-black Ni-P alloy was historically the best ultra-black material until the advent of low-dimensional carbon technologies. It is still widely used in industry [9]. Graphitic materials have been regarded as an effective material in conventional black paintings owing to their strong absorption of visible light due to the π band’s optical transition [10]. Carbon nanotube arrays, fabricated through a bottom-up process, can achieve almost perfect absorption in the wavelength range 0.2-200 μm [11]. Materials based on carbon nanotube arrays have been extensively developed for absorption applications [12–18]. Owing to their low material density of ~3% [18,19], impedance matching could be achieved at the interface between the carbon nanotube arrays and the environment. However, this is generally at the expense of material thickness and such absorbers are often hundreds of micrometers thick. Moreover, semiconductor or metal materials, which are relatively fragile and have lower melting points than carbon materials, are required for catalyzing synthesis of the carbon nanotubes, making these absorbers rigid and not appropriate for working at high temperature.

Recent studies have shown that modifying the surface of highly oriented pyrolytic graphite (HOPG) material with nanostructures (nanopillar, nanodisk, nanocone) through top-down approaches would lead to enhanced absorption in the visible and NIR ranges with structures thinner than 1 μm [20–22]. In such absorbers, large thickness and small tip size of the nanostructures were essential in reducing the reflection. As thin film HOPG is bendable, and HOPG material has a melting point higher than 3000 K [23], absorbers made from HOPG could be bendable and suitable for working at high temperature environments. However, there is still no feasible way to produce large area HOPG nanostructures with both sufficient thickness and sharp tips. The lowest reflectance realized by such approaches is ~10% [20], which is still not comparable to the ultra-black carbon nanotube array materials, nor the Ni-P materials.

Here, we report a bendable ultra-black material made from pristine HOPG through a simple plasma etching process. This 5 μm HOPG absorber demonstrates broadband absorption comparable to bottom-up grown carbon nanotube materials in the visible and NIR ranges. According to calculation and simulations, high performance is ascribed to the synergy of the ultra-low surface reflectance of the nanowires and the highly efficient light absorption of the nanocones. Additionally, the HOPG absorber exhibits strong light absorption even when the angle of incidence (AOI) is 70°, regardless of polarization.

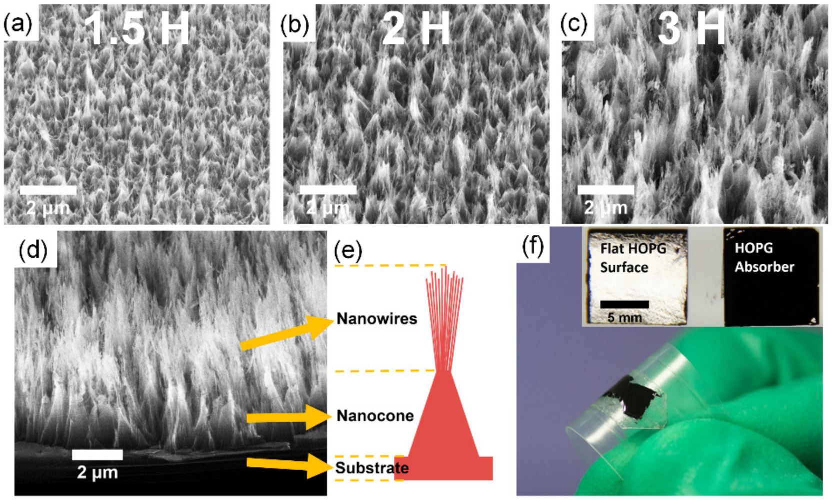

Fig. 1. The 45° tilted view scanning electron micrograph (SEM) pictures of the HOPG absorber samples as a function of etching time: (a) 1.5 H, (b) 2 H, and (c) 3 H. (d) A side view SEM picture of sample 3 H. (e) A schematic of the elementary nanostructure of the HOPG absorber composed of nanowires, a nanocone, and the substrate. (f) A photograph of a piece of HOPG absorber peeled off from the substrate and pasted on a bendable transparent plastic film. The inset shows a photograph of a flat HOPG surface and an HOPG absorber.

2. Fabrication and SEM characterization

The HOPG absorber is fabricated using a simple three-step inductively coupled plasma (ICP) etch process on the HOPG substrate (10 × 10 × 1 mm, B class, Nanjing XFNANO Materials Tech Co., Ltd.), covered with spin coated 1.1 μm photoresist film (AZ 5214E, Clarient Co.). The three etching steps consist of a 1 minute oxygen plasma etch to reduce the thickness of the photoresist film, a 3.5 minute CHF_3 and CF_4 plasma etch to roughen the surface of the photoresist film, and a 1.5-3 hour oxygen plasma etch to form the graphite nanostructures of

#242069 Received 1 Jun 2015; revised 20 Jul 2015; accepted 21 Jul 2015; published 24 Jul 2015
© 2015 OSA

the HOPG absorber. By varying the time duration (1.5, 2, and 3 hours) of the last step in the fabrication process, three HOPG absorbers with different nanostructure sizes were obtained (samples 1.5 H, 2 H, and 3 H). The 45° tilted view SEM micrographs of the samples, presented in Figs. 1(a)-1(c), indicate that the average heights and widths of the nanostructures increase with increased etching time.

As shown in the side view of the sample 3 H in Fig. 1(d), the HOPG absorber is composed of randomly distributed nanocones in the bottom layer with nanowires on top, and the bulk HOPG substrate beneath both layers. The elementary nanostructure is illustrated in Fig. 1(e). The nanowires and nanocone have almost equal heights. And the average total height of the nanostructures of the HOPG absorber sample 3 H is around 4.5 μm, which is only around half of the thickness of the ultra-thin carbon nanotube absorber (<10 μm) [24]. The nanocones have cone angles ~40° and top diameters ~300 nm. The nanowires are protruding from the top of the nanocones vertically, with deviation angles generally less than 10°. Since pristine HOPG material has layer structures stacked in the direction normal to its surface plane, the nanowire structures etched out from it are mostly composed of stacked graphite layers rather than standing graphite rolls as in carbon nanotubes.

The HOPG absorber is sufficiently thin to be transferred to a bendable surface as demonstrated in Fig. 1(f). By pressing a piece of adhesive tape to a small region at a corner of the sample's surface, a large piece of HOPG absorber can be gently peeled off from the substrate. The back of the HOPG absorber is then pasted on the surface of a piece of bendable plastic film with a piece of double-sided tape. Since most surface area of the HOPG absorber was not touched by anything during this process, it remains black after the transfer. The inset of Fig. 1(f) shows a photograph of the HOPG absorber in comparison to a flat HOPG surface. The HOPG absorber exhibits good uniformity over the 1 cm^2 sample surface and a very high level of absorption across the visible spectral range.

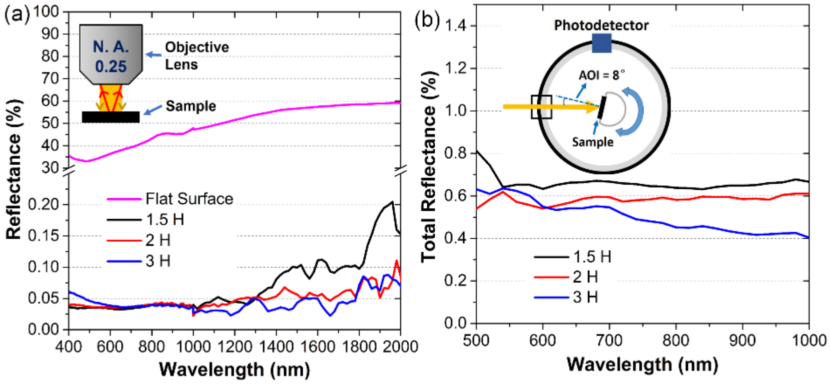

Fig. 2. (a) The measured specular reflectance of HOPG absorber samples 1.5 H, 2 H, and 3 H along with a flat HOPG surface in the wavelength range of 400-2000 nm. The inset schematically depicts the set-up of the specular reflectance measurement. (b) The measured total reflectance of HOPG absorber samples 1.5 H, 2 H, and 3 H in the wavelength range of 500-1000 nm. The inset illustrates the set-up for the total reflectance measurement.

3. Measurement and analyses

The specular reflectance of the three HOPG absorber samples 1.5 H, 2 H, and 3 H along with a flat HOPG surface are presented in Fig. 2(a). The measurements are conducted with a homemade reflective microscope [25] shielded by a black curtain. The sample is illuminated by unpolarized normal incident light from a Zolix LSH-T75 halogen lamp through a 10 × objective (N.A = 0.25) under Kohler condition, as depicted in the inset of Fig. 2(a). The reflected light is collected with the same objective and then passes through a square aperture with side length of 100 μm, which minimizes the stray light that can reach the detector. The

Received 1 Jun 2015; revised 20 Jul 2015; accepted 21 Jul 2015; published 24 Jul 2015
© 2015 OSA

visible wavelength (400-1000 nm) is measured directly by an Ocean Optics USB2000 spectrometer, while the longer wavelength (1000-2000 nm) is measured with a Zolix Omni-λ1509 monochromater and Zolix DInGaAs 2600-TE detector. The reflecting power from an Ideaoptics STD-M aluminum mirror, which have an average reflectivity of ~95% in the wavelength range of 400-2000 nm, is measured as the reference signal. The reflecting power of the sample is then measured and normalized to the reference signal.

From Fig. 2(a), we can see that all three of the HOPG absorber samples show ultra-low reflectivity in the wavelength range 400-2000 nm. The specular reflectance of the samples is as low as 0.035% in the visible range, nearly 3 orders of magnitude lower than the unmodified flat HOPG surface. The specular reflectance of samples 2 H and 3 H averages below 0.05% from 400 nm to 2000 nm. The samples with longer etch time have relatively lower reflection in the NIR range.

The uncertainty of the specular reflectance measurements mostly comes from the relatively low signal-to-noise ratio of the detection equipments for weak reflection signals. The signal-to-noise ratio of the sample measurements ranges from 30:1 to 5:1 in the visible range, and ranges from 5:1 to 2:1 in the NIR range. The signal-to-noise ratio of the reference measurement is well above 100:1 across visible to NIR range. The relative uncertainties due to the optical instability of the tungsten lamp and the imperfect reflection of the aluminum mirror are ~1% and ~5%, respectively. Therefore, the average specular reflectance results in the wavelength range of 400-2000 nm have an expanded uncertainty of ~0.03%, with a coverage factor of $k = 1$.

The total reflectance of the HOPG absorber samples was measured with an integrating sphere system (QTest Station 1000, CrownTech) in the wavelength range of 500-1000 nm. The integrating sphere system consists of a tungsten lamp, a monochromator, an SR830 lock-in amplifier (Stanford Research Systems), a NIST traceable Si detector (Hamamatsu), and a sample chamber enclosing an integrating sphere and the optical alignment setup. As depicted in the inset of Fig. 2(b), the sample is mounted to a rotary holder in the center of the integrating sphere for adjusting the angle of incidence (AOI) of the measurements. Specifically, the near-normal-incidence data are measured at AOI = 8° to avoid the loss of the specular reflection signal. The illumination area on the sample is ~1 mm × 2 mm. A Si detector is positioned on the wall of the integrating sphere to collect the redistributed signal of the reflected light from the sample. The reference signal is measured with a Polytetrafluoroethylene (PTFE) standard, whose reflectivity is above 99% in the wavelength range of 350-1800 nm. The reflecting power of the sample is then measured and normalized to the reference signal.The polarization-dependent measurements (TE, TM) were conducted by inserting a polarizer (Union Optic, SHP0025) in the incident light path. The TE polarization is defined as the electric field parallel to the surface plane of the sample.

As shown in Fig. 2(b), the total reflectance of the HOPG absorber samples demonstrate a trend similar to the specular reflectance trend – the sample with the longest etch time has the lowest reflectance in the NIR range, but increase at the UV end. This is typical behaviour of carbon nanowire growth. The hemispherical reflectance of samples 2 H and 3 H are below 0.7% over the entire measured wavelength range, and further, sample 3 H demonstrates low total reflectance of ~0.4% at λ = 1000 nm. Our samples are half the thickness of the ultra-thin carbon nanotube absorbers fabricated from a bottom-up method having a total reflectance of 1.8% at λ ~1000 nm [24].

The signal-to-noise ratios of the measurements of the total reflectance of the samples and the reference are ~20:1 and above 1000:1, respectively. The stray light from the single monochromator is less than 10^{-4}. The relative uncertainties due to the optical instability of the tungsten lamp and the imperfect reflection of the PTFE standard are <0.15% and <1%, respectively. Therefore, the total reflectance results of samples 2 H and 3 H have an expanded uncertainty of ~0.07%, with a coverage factor of $k = 1$.

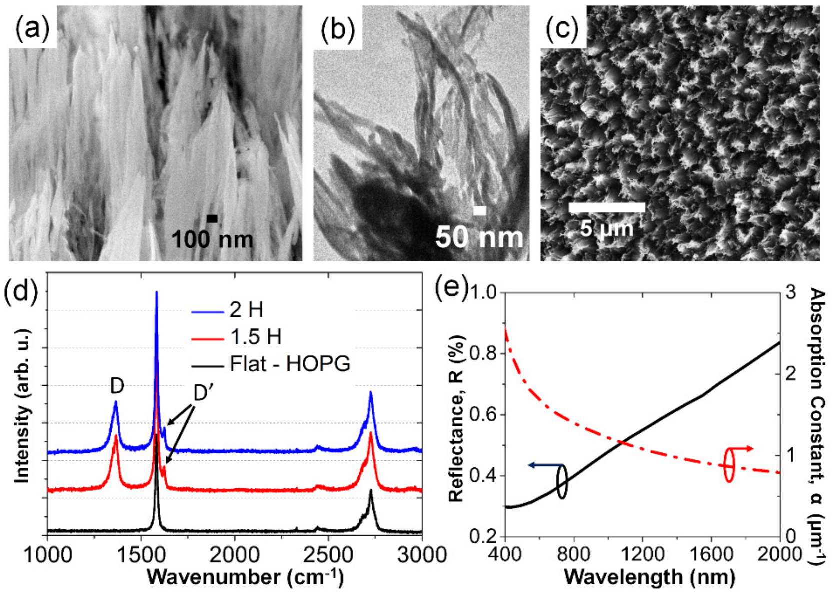

Fig. 3. (a) Side view SEM and (b) TEM pictures of the tips of the nanowires of HOPG absorber sample 3 H, indicating that the nanowires have diameters mostly in the range of 20-100 nm. (c) A top view SEM picture of HOPG absorber sample 3 H. (d) Raman Spectra taken for sample 2 H, 1.5 H and a flat HOPG surface. (e) The calculated surface reflectance (solid curve) and the effective absorption constant (dash-dotted curve) of the nanowires.

The ultra-blackness of the thin HOPG absorber is ascribed to two major factors: the near-zero reflectance at the surface of the nanowires and the efficient absorption brought by the nanocones.

The near-zero reflectance at the surface of the HOPG absorber can be explained by impedance matching of the nanowires [18]. A side view SEM and a TEM picture of the HOPG absorber sample 3 H, presented in Figs. 3(a) and 3(b), show the sharp tips of the nanowires. No obvious object other than the graphite nanostructures is observed in Figs. 3(a) and 3(b), the broken parts of the nanowires in Fig. 3(b) are due to the process in the preparation of the TEM specimen. The diameters of the nanowires mostly fall in the range of 20-100 nm, well below the wavelengths of interest, thus an effective medium treatment is reasonable [26]. According to the top view SEM picture of the HOPG absorber sample 3 H shown in Fig. 3(c), the regions representing the top of the nanowires have the brightest signals. The filling factor of the nanowires could therefore be estimated as the proportion of the brightest areas, which is around 5%. The Raman spectra of pristine HOPG and samples 1.5 H and 2 H excited with a 514 nm wavelength Ar ion laser are presented in Fig. 3(d). The most prominent feature of the Raman spectra of the nanostructured samples is the appearance of the D (~1350 cm^{-1}) and D' (1620 cm^{-1}) peaks, which indicates the increase of structural disorder of graphite material [20, 27, 28]. Therefore it is reasonable to assume that the material of the fabricated samples is predominantly HOPG, and the possible products of the photoresist material can be neglected in the analysis. According to the effective medium theory, the effective refractive index ($\tilde{n}_{eff}$) of the nanowires can be calculated by using the weighting formula [29,30]:

$$\tilde{n}_{eff} = ff \cdot \tilde{n}_g + (1 - ff) \cdot \tilde{n}_0 \qquad (1)$$

where ff is the filling factor of the nanowires, and $\tilde{n}_g$ and $\tilde{n}_0$ are the complex refractive indices of graphite [31] and air, respectively. We use ff = 5% for the calculation of $\tilde{n}_{eff}$ in the wavelength range of λ = 400-2000 nm. In Fig. 3(e), we plot both the surface reflectance (R) calculated according to Fresnel's law and the absorption constant (α) obtained from the imaginary part of $\tilde{n}_{eff}$ for light normally incident onto the surface of the nanowires. Owing to the relatively low ff , R is low over the entire wavelength range of calculation, showing the good anti-reflection property of the nanowires. However, the relatively low α indicates that the nanowires alone could not achieve sufficient absorption with thin structure thickness (i.e. 4.5 μm), especially at longer wavelengths.

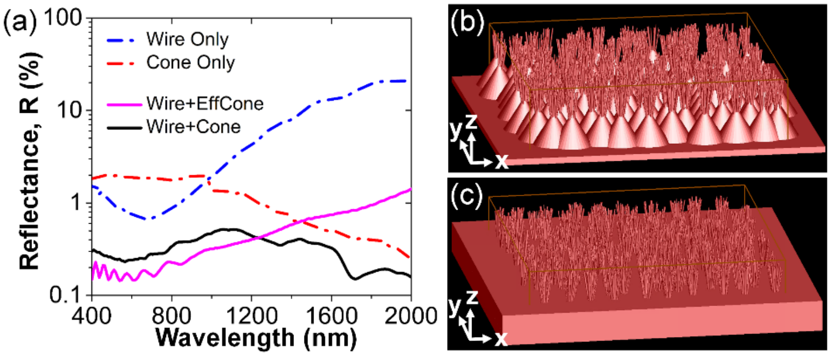

Fig. 4. (a) The simulated reflection spectra of four models that compare the functions of the different parts of the absorber. The 3D FDTD simulation models for (b) the nanowire + nanocone structure, and (c) the nanowire + effective media with tapered optical constant structure.

To further investigate the function of different parts of the HOPG absorber, we built four models composed of nanostructures for three-dimensional finite difference time domain (3D FDTD) analysis (Lumerical Software). The simulated reflectance spectra for TE polarized (electric field polarized in the x direction) normal incident plane wave light are presented in Fig. 4(a). As shown in Figs. 4(b) and 4(c), the nanostructures are randomly placed in the 12 μm × 12 μm simulation regions included in the orange boxes. The random positions and sizes of the nanostructures are generated by the embedded script language of the Lumerical FDTD Solution software. Periodic conditions are applied along the x- and y- boundaries of the models, and perfectly matched layer boundary conditions are applied along the z- boundaries of the models.

The blue curve corresponds to a model composed of 4.5 μm long nanowires with random diameters in the range of 20-100 nm on a 500 nm thick HOPG substrate. An overall ff of ~5% is achieved with 2520 nanowires. As a supplement to the effective medium theory analysis, multiple scattering effect is included in the 3D FDTD simulation. The reflectance of this model is relatively low over the visible range and rises across the NIR range. In the wavelength range of 1600-2000 nm, the simulated reflectance is even higher than 10%, indicating strong reflection occurs at the interface between the nanowires and the HOPG substrate. This result supports the conclusion of the $\tilde{n}_{eff}$ analysis that the 4.5 μm long nanowires cannot achieve sufficient absorption by themselves.

The red curve corresponds to a model composed of 120 nanocones on a 500 nm thick HOPG substrate. The nanocone in a unit cell has a height of 2.25 μm, a top diameter of 300 nm, a base diameter of ~1.9 μm and a cone angle of 40°. The mean spacing between adjacent unit cells is ~1.2 μm. This model shows an average reflectance level around 1%, indicating the nanocones could realize highly efficient absorption. Previous studies have shown that cones can provide efficient anti-reflective properties due to the gradient index of refraction (GRIN) [32–34] and a relatively large overall absorption constant. As the characteristic scales (i.e. base diameter, mean spacing) of the nanocones are larger than the wavelength of visible

#242069
Received 1 Jun 2015; revised 20 Jul 2015; accepted 21 Jul 2015; published 24 Jul 2015
© 2015 OSA

light, the incident visible light will be reflected and scattered partly, and thus results in the relatively high reflectance of the red curve in the visible wavelength range. This reflection and scattering is reduced when wavelength is comparable to the characteristic scales of the nanocones, resulting in a decreased reflectance in the NIR wavelength range.

The black and pink curves correspond to two different models of the HOPG absorber, which are depicted in Figs. 4(b) and 4(c), respectively. The model of the black curve is composed of 120 nanowire nanocone composite structures on a 500 nm thick HOPG substrate. The unit cell of this model has 21 nanowires with lengths of 2.25 μm protruding from a 2.25 μm tall nanocone with deviation angles less than 10°. The geometrical parameters of the nanowires and the nanocone are the same as the previous models correspond to the blue and red curves, respectively. This model shows the importance of both impedance matching provided by the nanowires at the surface and the efficient absorption provided by the nanocones at the bottom, with a similar GRIN profile as in ref [32,33]. The black curve demonstrates much lower reflectance than the blue and red curves and has an average level lower than 0.4%, showing the synergy of the nanowires and nanocones can significantly enhance the absorption efficiency in a broad wavelength range of $\lambda = 400$-2000 nm.

The model of the pink curve is similar to the model of the black curve, except that multi-layer effective media, which have optical constant values gradually increase from the top to the bottom, are used in replace of the nanocones. The discrepancy between the black and the pink curves occurs at the NIR range, indicating that the incident NIR light will be trapped in the gaps of the nanocones which have characteristic scales similar to the wavelength, leading to enhanced light-matter interaction and absorption efficiency [26].

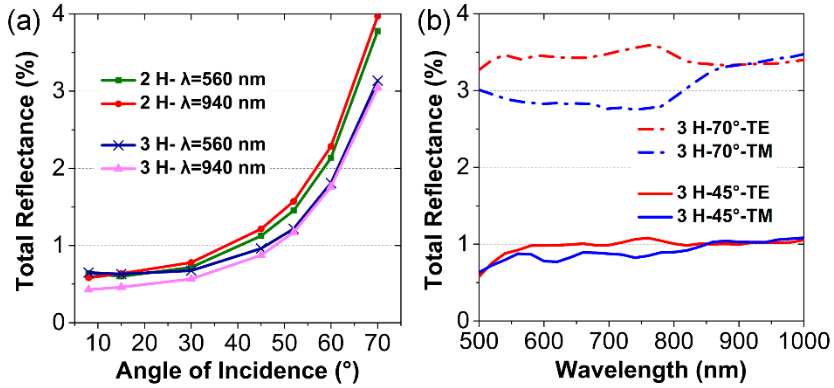

Fig. 5. (a) A plot of measured total reflectance as a function of AOI for samples 2 H and 3 H at wavelengths of 560 nm and 940 nm. (b) The small polarization dependence (TE and TM polarizations) of the measured total reflectance of sample 3 H at large AOIs of 45° and 70° in the wavelength range of 500-1000 nm.

The dependency of the total reflectance on the AOI of the HOPG absorber samples 2 H and 3 H are presented in Fig. 5(a). The total reflectance of the two HOPG absorber samples at the wavelengths $\lambda = 560$ nm and $\lambda = 940$ nm is shown to increase monotonically with increasing AOI, and the curves become steeper at larger AOI. The HOPG absorber sample 3 H has the best performance at larger AOI, and its total reflectance remains below 3.5% even when the AOI is as large as 70°. We also studied the polarization-dependence of the HOPG absorber sample 3 H at large AOIs (i.e. 45° and 70°). According to Fig. 5(b), although the polarization dependence is larger when AOI is 70°, the difference in the reflectance due to the polarizations remains well below 25% of the average reflectance of the two polarizations, showing that this material is capable of working as the absorbing device for all polarizations.

#242069 Received 1 Jun 2015; revised 20 Jul 2015; accepted 21 Jul 2015; published 24 Jul 2015
© 2015 OSA

4. Conclusion

In summary, we have experimentally demonstrated that a 5 μm thin and bendable HOPG absorber composed of nanocone and nanowire composite structures, made using a top-down method, can exhibit ultra-low specular reflectance (~0.05 ± 0.03%) and total reflectance (~0.5 ± 0.07%) over a wide spectral range from the visible to NIR. The unique properties of this HOPG absorber are ascribed to the impedance matching provided by the nanowires at the surface, and the efficient light-matter interaction provided by the nanocones. Analyses based on effective medium theory and 3D FDTD simulations were conducted to substantiate these conclusions. Moreover, this material is capable of working at large AOI and is insensitive to polarization, making it very promising for applications such as solar energy collectors, thermal sensors, and stray light shields in optical systems.

Acknowledgment

The authors acknowledge the partial support of the National Natural Science Foundation of China (Nos. 91233208, 61178062, and 61271016), the National High Technology Research and Development Program (863 Program) of China (No. 2012AA030402), the program of Zhejiang Leading Team of Science and Technology Innovation (2010R50007), Swedish VR grant (# 621-2011-4620) and AOARD. We thank Lei Mo for technical assistance on the specular reflectance measurements, Bin Shi for support in SEM characterization, Xianhe Sun for support in Raman characterization, and Prof. Yungui Ma and Prof. Yi Jin for fruitful discussions.